Controlling fingering instabilities in rotating ferrofluids

David P. Jackson
Department of Physics and Astronomy, Dickinson College, Carlisle, Pennsylvania 17013

José A. Miranda
Laboratório de Física Teórica e Computacional, Departamento de Física, Universidade Federal de Pernambuco, Recife, PE 50670-901 Brazil

(Received 25 July 2002; published 24 January 2003)

We perform a detailed analytic and numerical study of the evolution of a ferrofluid drop confined to a rotating Hele-Shaw cell in the presence of an azimuthal magnetic field. Our results demonstrate that the centrifugally driven interfacial instabilities can be simply controlled with the use of a current-carrying wire. We compare an analytic linear analysis to our computational results and show that a number of observed features cannot be explained by linear theory alone, including a ''diamond ring'' instability that results when a droplet is nearly stabilized.

DOI: 10.1103/PhysRevE.67.017301 PACS number(s): 47.54.+r, 75.50.Mm, 47.20.−k, 47.20.Ma

The shape evolution of a rotating liquid drop has been a subject of long-standing interest due to its relation to a wide variety of phenomena ranging from nuclear fission to planetary motion [1]. The related phenomenon of *spin coating*—the flow of a thin pool of liquid spreading on a rotating horizontal surface—is also a topic of considerable scientific and practical importance [2–4]; it occurs in a number of technological applications such as the manufacture of magnetic storage disks and the application of photoresist in microcircuit fabrication.

Centrifugally driven flows involve the development of hydrodynamic instabilities. As a thin, rotating liquid droplet spreads over a solid substrate, its boundary becomes unstable and develops undulations that eventually grow into complex fingerlike interfacial patterns. Experimental studies reveal the occurrence of fingering instabilities in the spreading of both free and confined thin liquid films. In free surface flows, the development of nearly polygonal structures whose vertices eventually break into long radially outgoing fingers is observed [5,6]. Confined flows in Hele-Shaw cells exhibit a different kind of fingering structure in which the central initial drop throws out attached droplets, which themselves form new droplets [7]. Despite their interesting morphologies and rich dynamical behavior, these patterned structures are typically undesirable in technological applications since they can result in uneven surface coverage. Thus, it is important to develop a fundamental understanding of the dynamics of these systems, and to find ways to control such hydrodynamic instabilities.

In this paper we focus on an initially circular droplet of a magnetic fluid (ferrofluid) in a rotating Hele-Shaw cell. Ferrofluids are colloidal suspensions of nanometer-sized magnetic particles suspended in a nonmagnetic carrier fluid. These fluids behave superparamagnetically and can easily be manipulated with external magnetic fields that can act to either stabilize or destabilize the fluid interface [8]. Examples of destabilization include the so-called Rosensweig or normal-field instability—in which an initially flat free surface evolves into a hexagonal pattern of peaks, and the labyrinthine instability—in which a ferrofluid confined to a Hele-Shaw cell evolves into a very intricate, mazelike structure. Examples of stabilization include the elimination of the Kelvin-Helmholtz instability and suppression of the fingering instability in flow through porous media.

Recently, a linear analysis demonstrated that a particularly simple magnetic field configuration, produced by a current-carrying wire, was capable of stabilizing the interface of a confined, rotating ferrofluid drop [9]. Here, we extend those results and provide a quantitative investigation of the system in both the linear and nonlinear regimes. Consider a Hele-Shaw cell of thickness b containing two immiscible, incompressible, viscous fluids with interfacial surface tension σ (see Fig. 1).

Denote the densities and viscosities of the inner and outer fluids, respectively as ρ_1, η_1 and ρ_2, η_2. We assume that the inner fluid is the ferrofluid while the outer fluid is nonmagnetic. The Hele-Shaw cell rotates with constant angular velocity Ω about an axis perpendicular to the plane of the flow and a long straight current-carrying wire is directed along the axis of rotation. The magnetic field produced by the wire is $\mathbf{H}=I/(2\pi r)\,\hat{\mathbf{e}}_\theta$, where r is the distance from the wire and $\hat{\mathbf{e}}_\theta$ is a unit vector in the azimuthal direction. Note that the azimuthal symmetry and radial gradient of the magnetic field will result in a magnetic force directed radially

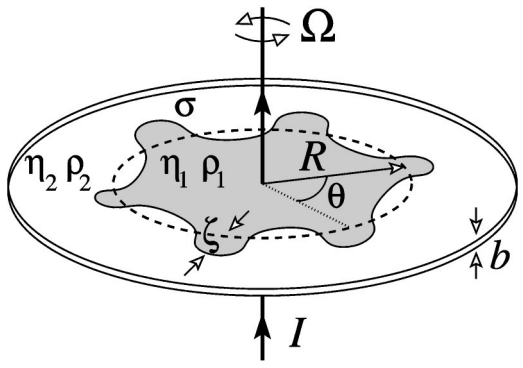

FIG. 1. A ferrofluid drop in a rotating Hele-Shaw cell; a current-carrying wire is aligned with the axis of rotation.

inward. This is exactly what is needed to stabilize the outward centrifugal force.

To study the hydrodynamics of rotating ferrofluids, the usual Navier-Stokes equation is modified through the inclusion of terms representing magnetic and centrifugal forces. We assume that the ferrofluid is uniformly magnetized and that **M** is collinear with the external field **H** [10–12]. For the quasi-two-dimensional geometry of a Hele-Shaw cell, we reduce the three-dimensional flow to an equivalent two-dimensional flow $\mathbf{v}(r,\theta)$ by averaging over the z direction. Using a parabolic velocity profile with no-slip boundary conditions and neglecting inertial terms (including the Coriolis force), one derives Darcy's law for ferrofluids in a rotating Hele-Shaw cell as [9]

$$\mathbf{v}=-\frac{b^2}{12\eta}\nabla\Pi, \tag{1}$$

where the generalized pressure Π consists of the z-averaged hydrodynamic pressure $1/b\int p\,dz$, plus magnetic $\frac{1}{2}\mu_0\chi H^2$ and centrifugal $\frac{1}{2}\rho\Omega^2 r^2$ terms. Here, μ_0 is the free-space permeability and χ is the constant magnetic susceptibility. Equation (1) describes nonmagnetic fluids by simply dropping the magnetic term.

We take the initial state of the interface to be a circle of radius R. Then, in the framework of linear analysis, we describe the interface in polar coordinates as $\mathcal{R}(\theta,t)=R+\zeta(\theta,t)$, and consider a small perturbation of the form $\zeta(\theta,t)=\zeta_n(t)\exp(in\theta)$, where $n=1,2,3,\ldots$. The problem is then specified by two boundary conditions: (i) the pressure jump at the interface $(\Pi_1-\Pi_2)|_{\mathcal{R}}=\sigma\kappa|_{\mathcal{R}}$, where κ denotes the interface curvature; and (ii) the kinematic boundary condition $\mathbf{n}\cdot\nabla\Pi_1|_{\mathcal{R}}=\mathbf{n}\cdot\nabla\Pi_2|_{\mathcal{R}}$, where $\mathbf{n}$ is the unit normal vector pointing from fluid 1 to fluid 2. Following the usual linear stability procedures, we obtain the differential equation for the Fourier perturbation amplitudes $\dot{\zeta}_n=\lambda(n)\zeta_n$, where

$$\lambda(n)=\frac{b^2\sigma n}{12(\eta_1+\eta_2)R^3}[N_\Omega-N_B-(n^2-1)] \tag{2}$$

is the linear growth rate. Here, we have defined $N_\Omega=[R^3(\rho_1-\rho_2)\Omega^2]/\sigma$ and $N_B=\mu_0\chi I^2/(4\pi^2\sigma R)$ as the (dimensionless) rotational and magnetic bond numbers, respectively. Since a positive growth rate leads to an unstable interface, Eq. (2) tells us that since N_B is always positive, the magnetic field will always stabilize the interface. On the other hand, N_Ω can be either positive or negative depending on whether the inner or outer fluid is more dense. Thus, the centrifugal force can be either stabilizing or destabilizing.

Some important information can be extracted from the linear growth rate. The first is the neutral stability curves [for which $\lambda(n)=0$]

$$N_\Omega=N_B+(n^2-1), \tag{3}$$

which determine when a particular mode becomes unstable. When $N_B=0$, the mode $n=1$ is unstable for any value of $N_\Omega>0$ and higher modes become unstable for $N_\Omega>n^2-1$.

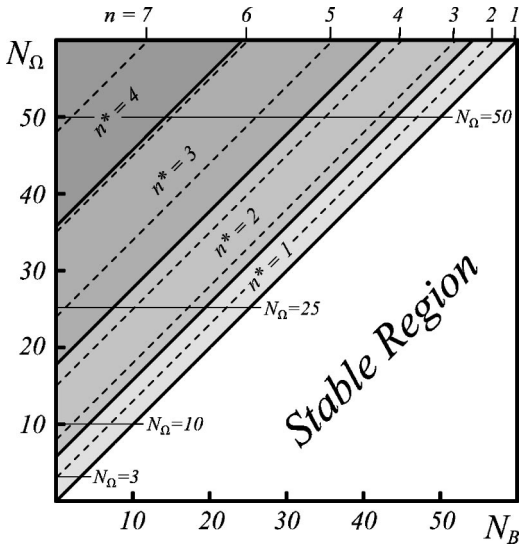

FIG. 2. Linear stability phase plot showing neutral stability curves (dashed) and zones (shaded) of fastest growing mode n^*. Horizontal lines give values of N_Ω used in the simulations.

We also note that for a particular value of N_Ω, increasing N_B stabilizes more and more modes until $N_B=N_\Omega$, at which point *all* modes are stable. Thus, we should see no evolution under these conditions.

Another useful quantity that linear theory gives us is the fastest growing mode n^*, defined as the (integer) mode that produces the largest growth rate. This is the mode that will tend to dominate during the early stages of the pattern formation process and will perhaps determine the number of fingers in the final state. Now, a given mode n is only the fastest growing when $\lambda(n)>\lambda(n-1)$ and $\lambda(n)>\lambda(n+1)$. Using Eq. (2), we find that the boundaries of the region dominated by a particular mode is given, for integer n, by

$$N_\Omega=N_B+3n(n\pm1). \tag{4}$$

Again, one can see that for a given N_Ω, increasing N_B will tend to decrease the number of fingers that develop.

Figure 2 depicts a ''phase diagram'' in N_Ω-N_B parameter space for the linearized system. The dividing line $N_\Omega=N_B$ separates the stable and unstable regions of the phase diagram, and represents the neutral stability curve for mode $n=1$. Thus, as long as $N_B\geqslant N_\Omega$, we are within the stable region and should observe an unchanging circular droplet centered on the axis of rotation. As one moves further into the unstable region, the dashed lines represent the boundaries where higher modes n (labeled on the top of the graph) become unstable as given by Eq. (3). The solid lines that encompass the shaded regions, determined from Eq. (4), denote zones where a particular mode is the fastest growing and are labeled n^* on the graph.

As an example of how one might use this graph, consider the case where $N_\Omega=50$ is held fixed. When $N_B=0$, modes 1–7 are all unstable even though we are in a zone of $n^*=4$. Therefore, one might expect that all else being equal, an initially circular droplet would develop into a four-fingered structure. As N_B is increased, the higher modes become sta-

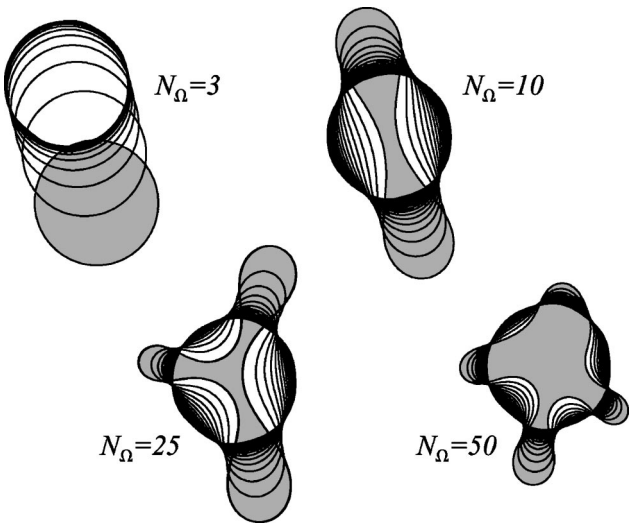

FIG. 3. Equally spaced time steps overlaid to show the evolution of a rotating ferrofluid drop with no magnetic field; larger N_Ω represents higher rotation rate.

bilized and the fastest growing mode also decreases. Note, however, that a particular mode remains unstable long after losing its status of fastest growing mode.

Finally, we note that in contrast to the usual viscous fingering problem in nonrotating Hele-Shaw cells [13], the Fourier mode $n=1$ that corresponds to a rigid translation of an unperturbed circular droplet can become unstable for flows in rotating cells. This is because the instability is driven by a viscosity difference in one case and a density difference in the other. In Fig. 2, the unstable zone labeled by $n^*=1$ would be related to such interesting dynamical behavior.

To test the predictions from linear theory and also to examine the long time behavior of this system far into the nonlinear regime, we perform a series of numerical experiments. We take the simplest situation in which the outer fluid has negligible viscosity and density and assume the hydrodynamic pressure is a constant. Since the ferrofluid is incompressible, $\nabla\cdot\mathbf{v}=0$ and Eq. (1) reduces to a Dirichlet problem for an arbitrarily shaped simply-connected domain. Since the Dirichlet problem on the unit disk is known, we use a conformal mapping technique to map that solution to the domain of interest [14,15]. Using this approach, the interface is given by the complex function $\rho(\alpha)$ and evolves according to

$$\partial_t\rho = i(\partial_\alpha\rho)\mathcal{A}\left\{\frac{\mathrm{Re}[z\partial_z\mathcal{A}\{\Pi\}]_{e^{i\alpha}}}{|\partial_\alpha\rho|^2}\right\}_{z=e^{i\alpha}}, \qquad (5)$$

where α parametrizes the interface. Here, the integral operator $\mathcal{A}$ takes a real function $\Pi(\alpha)$ and returns a function that is analytic inside the unit disk whose real part evaluated at $e^{i\alpha}$ is $\Pi(\alpha)$. For the results presented in this paper, all experiments begin with the same initial state of a circle centered on the axis of rotation with a small amount of random noise distributed in the first eight azimuthal modes. Note also that the data are presented as seen in the rotating frame of reference in which the Hele-Shaw cell appears stationary.

We begin our numerical experiments by first considering rotations alone ($N_B=0$). Figure 3 shows time overlaid plots illustrating the evolution for rotation numbers $N_\Omega=3$, 10, 25, and 50. The initial state is the same in each case and the experiments were stopped before the complicated ''pinch-off'' process [16]. For clarity, the final shapes have been shaded, but it is important to note that these are *not* equilibrium states. In addition, while the time steps are equally spaced, the total time is different for each experiment. The larger the centrifugal effects, the smaller the time required to reach pinch off.

One can immediately notice that higher rotations lead to more fingered structures. In fact, the simulations beautifully capture the rigid translation of the drop for small N_Ω. Although this rigid translation is expected from linear theory, it is a bit surprising that the droplet maintains its shape as it moves far off axis. A noteworthy point is that the observed number of fingers for the patterns depicted in Fig. 3 agrees precisely with the fastest growing mode from the linear analysis. As shown in Fig. 2, when $N_B=0$, rotation numbers of $N_\Omega=3$, 10, 25, and 50 lie in the zones $n^*=1$, 2, 3, and 4, respectively. This suggests that linear theory is a good predictor of the final number of fingers, at least, when there is no magnetic contribution. While one might expect this agreement if the initial state is such that each mode has the same amplitude, it is important to question the role of the initial conditions. As already mentioned, our initial circles were sprinkled with a small amount of random noise, but what if the initial condition was such that a particular mode had a

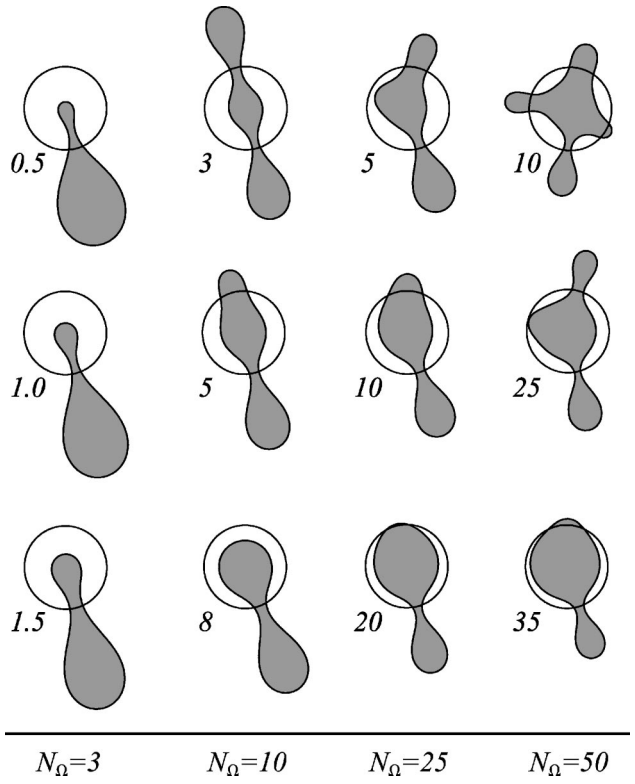

FIG. 4. The effect of nonzero magnetic field on the evolutions shown in Fig. 3. Only the initial circle and final state (shaded) are shown; N_B is listed next to each simulation.

larger amplitude than the others? Would that affect the pattern formation process?

To answer this question, we ran a number of simulations with an initial perturbation consisting of a single mode. This state was then used in experiments with various combinations of N_Ω and N_B and we looked at the resulting evolution. We found that as long as a particular mode was unstable, then an initial condition of that mode led to a structure with the same number of fingers regardless of what the fastest growing mode was. For example, an initial state of mode $n=3$ led to a three-fingered structure as long as we were above the mode-3 instability line ($n=3$ dashed line) in Fig. 2. This tells us that the initial conditions can play a very important role in the pattern formation process. On the other hand, if the initial conditions are such that there is no mode preference, we should expect n^* to be a reasonable predictor of the number of fingers in the final structure.

Figure 4 shows the effect of an external azimuthal magnetic field on the evolutions shown in Fig. 3. The columns in Fig. 4 are arranged according to N_Ω (labeled at the bottom) and in each column, N_B (labeled next to each pattern) increases from top to bottom. In this figure, we show only the position of the initial circle and the final state before pinch off. The introduction of the magnetic field enriches the problem considerably and significantly changes the linear shape scenario. The magnetic field tends to attract the evolving ferrofluid droplet toward the current-carrying wire, and a whole different family of patterns arises. For example, when $N_\Omega=3$, the rigid translation from Fig. 3 is interrupted as a small piece of the circle appears to be pinned down by the current-carrying wire; the larger the magnetic field, the more of the drop seems to get pinned down by the wire. For $N_\Omega=10$, the two-fingered dumbbell from Fig. 3 has developed a bump in the middle that gets larger for larger magnetic field values. In all cases, it is clear that increasingly larger values of N_B progressively reduces the number of outgrowing fingers. Ultimately, when $N_B \geqslant N_\Omega$, we reach a state of complete stabilization where no evolution takes place.

Last, we point out that all patterns shown in Fig. 4 share a common, interesting feature. Before reaching complete droplet stabilization, one observes an almost stable circle, with only one finger protruding from it. We call this nonlinear phenomenon the ''diamond ring'' instability. To try to gain some insight into this interesting behavior, we note from Eq. (3) that for $N_\Omega \leqslant N_B+3$, the only (possible) unstable mode is $n=1$. A careful study of the simulations in this region demonstrates that the initial circle first begins to undergo a rigid translation but then quickly develops a point of leakage at the spot furthest from the axis of rotation. This leakage point then gets pinched off resulting in what looks a bit like a diamond ring (particularly for faster rotations). This is an intrinsically nonlinear instability that is not predicted by linear theory. Therefore, we see that the introduction of the magnetic field does more than to effectively reduce the angular velocity of the cell. On the contrary, the interaction of the centrifugal and magnetic effects results in some interesting new behaviors and patterns.

We would like to thank the Brazilian Research Council-CNPq (J.A.M.), Santa Clara University, and Dickinson College (D.P.J.) for financial support of this research.

[1] N. Bohr and J.A. Wheeler, Phys. Rev. **56**, 426 (1939); S. Cohen, R. Plasil, and W.J. Swiatecki, Ann. Phys. (N.Y.) **82**, 557 (1974); R.A. Brown and L.E. Scriven, Proc. R. Soc. London, Ser. A **371**, 331 (1980).
[2] K.J. Ruschak, Annu. Rev. Fluid Mech. **17**, 65 (1985).
[3] N. Fraysse and G.M. Homsy, Phys. Fluids **6**, 1491 (1994).
[4] A. Oron, S.H. Davis, and S.G. Bankoff, Rev. Mod. Phys. **69**, 931 (1997).
[5] L.H. Tanner, Recherche **174**, 182 (1986).
[6] F. Melo, J.F. Joanny, and S. Fauve, Phys. Rev. Lett. **63**, 1958 (1989).
[7] Ll. Carrillo, F.X. Magdaleno, J. Casademunt, and J. Ortín, Phys. Rev. E **54**, 6260 (1996).
[8] R.E. Rosensweig, *Ferrohydrodynamics* (Cambridge University Press, Cambridge, 1985), and references therein.
[9] J.A. Miranda, Phys. Rev. E **62**, 2985 (2000).
[10] A.O. Tsebers and M.M. Maiorov, Magnetohydrodynamics (N.Y.) **16**, 21 (1980).
[11] A.O. Tsebers, Magnetohydrodynamics (N.Y.) **17**, 113 (1981).
[12] S.A. Langer, R.E. Goldstein, and D.P. Jackson, Phys. Rev. A **46**, 4894 (1992).
[13] L. Paterson, J. Fluid Mech. **113**, 513 (1981); K.V. McCloud and J.V. Maher, Phys. Rep. **260**, 139 (1995).
[14] D. Bensimon, L.P. Kadanoff, S. Liang, B.I. Shraiman, and C. Tang, Rev. Mod. Phys. **58**, 977 (1986).
[15] D.P. Jackson, R.E. Goldstein, and A.O. Cebers, Phys. Rev. E **50**, 298 (1994).
[16] R.E. Goldstein, A.I. Pesci, and M.J. Shelley, Phys. Rev. Lett. **75**, 3665 (1995).